PERGAMON

Electrochimica Acta 47 (2002) 1415–1422

ELECTROCHIMICA Acta

www.elsevier.com/locate/electacta

Electrochemical noise applied to the study of the inhibition effect of $CeCl_3$ on the corrosion behaviour of Al–Mg alloy AA5083 in seawater

A. Aballe, M. Bethencourt, F.J. Botana *, M. Marcos, R.M. Osuna

Departamento de Ciencia de los Materiales, Universidad de Cádiz, Ingeniería Metalúrgica y Química Inorgánica, Avda. República Saharaui s/n, CASEM, 11510 Puerto Real, Cádiz, Spain

Received 23 July 2001; received in revised form 6 November 2001

Abstract

Electrochemical noise measurements have been used to study the corrosion behaviour of aluminium alloy AA5083 in 3.5% NaCl solution with and without doping with $CeCl_3$ at 500 ppm. Information on the evolution of corrosion activity over a period of 4 days and on the corrosion mechanism itself has been obtained for the two systems. Experimental data obtained have been analysed using robust statistical parameters and wavelet transform; transient shapes were also studied. The various mathematical techniques applied to analyse the electrochemical noise data have been proposed recently. This paper thus not only characterises the corrosion systems studied but also illustrates the usefulness of these new methods.

Keywords: AA5083; Inhibition; Electrochemical noise; Corrosion; Cerium

1. Introduction

Type AA5083 aluminium alloy consists mainly of an aluminium matrix containing three kinds of intermetallic particles: Al(Mn, Fe, Cr), Al(Si, Mg) and Al–Mg [1]. The Al(Mn, Fe, Cr) particles have a major influence on the corrosion behaviour of the alloy in seawater, which is mainly characterised by three kinds of process:

- The development of a passive film overlying the aluminium matrix. This process involves the oxidation of atoms of the metal Al, which is an anodic reaction requiring a cathodic response to compensate for the excess of electrons produced. In this alloy, the 'consumption' of these electrons takes place preferentially on the Al(Mn, Fe, Cr) particles [2].
- *Alkaline pitting:* This pitting occurs as a consequence of the more cathodic nature of the Al(Mn, Fe, Cr) particles in comparison with the matrix of the alloy. Thus, since these intermetallic particles cause oxygen to reduce preferentially on them, there is a localised increase in pH in the zones surrounding these particles [3], which in turn causes the oxide layer in these areas to dissolve. As a result, the matrix is also attacked around the particles, causing a reduction of the contact between each particle and the matrix and, as a final stage, the physical detachment of the particles from the matrix, forming hemispherical pits [1,4].
- *Crystallographic pits:* These spread in a uniform manner according to the ⟨100⟩ crystallographic direction [5]. These pits only appear when the potential is above the pitting potential of the alloy. It has been found from potentiodynamic curves that this potential is −0.720 V versus an Ag/AgCl reference electrode [6].

Chromate-containing compounds are often used in protective pre-treatments of aluminium alloy surfaces. However, due to their high toxicity, more environment-friendly substitutes have been investigated [7]. In our laboratories, the effects of a variety of lanthanide chlorides have been studied, both as inhibitors of alloy AA5083 in seawater [8–10], and as components of conversion coatings for this system [11,12]. In these studies, the best inhibition behaviour was obtained

* Corresponding author. Tel.: +34-956-830-828; fax: +34-956-016-154.

E-mail address: javier.botana@uca.es (F.J. Botana).

0013-4686/02/$ - see front matter
PII: S0013-4686(01)00871-4

from the use of $CeCl_3$. It was observed that Ce^{3+} cations precipitate onto the Al(Mn, Fe, Cr) particles hindering the cathodic reaction from occurring [13].

The aim of the work described here is to extend the scope of the above-mentioned research by using electrochemical noise measurement (ENM). This technique has been chosen because it enables the system under study to be monitored continuously and without producing any alterations in the system. Thus, it is not necessary to conduct additional experiments to study the system behaviour for different exposure times. In addition, the analysis of the electrochemical noise (EN) provides information on both the corrosion kinetics and the mechanism of corrosion.

2. Experimental

2.1. Cell and corrosion systems

Samples of type AA5083 aluminium alloy (composition given in Table 1) were coated and mounted in epoxy resin. Since this kind of specimen often develops crevice corrosion, special care was taken to prevent it. Thus, cylindrical blanks were cut from plates made of AA5083 alloy. Then the blanks were coated so that one flat face with an area of 1 cm^2 was exposed to the solution, with an additional coating on the lateral surface of the blank. In addition, to obtain electrochemical measurements, an electrical connection was made on the back of each sample. Since two working electrodes (WEs) are used in ENM, two blanks were mounted in the same epoxy specimen, leaving a small gap between them. Once the epoxy specimen was ready, it was wet-abraded down to 1200 grade SiC finish and, afterwards, rinsed with distilled water. Thus, a cell consists of such a specimen immersed in a solution tank together with a 3 M Ag/AgCl reference electrode (−0.203 V vs. SHE) situated above the epoxy specimen, Fig. 1. In addition, a water jacket around the cell kept the temperature inside the cell at 30 °C throughout the experiments. To investigate the inhibitor effect of $CeCl_3$, two different media have been compared. One of these was artificial seawater (3.5% NaCl) while the other was prepared with NaCl and $CeCl_3$ so that the concentration of Cl^- was the same as the first solution and the concentration of Ce^{3+} was 500 ppm. This concentration of Ce^{3+} was chosen because it was found in previous studies [9] to provide the best performance for this system.

Table 1
Composition (wt.%) of the AA5083 Al–Mg alloy

Mg	Mn	Fe	Si	Cr	Cu	Ti	Al
4.9	0.5	0.3	0.13	0.13	0.08	0.03	Remainder

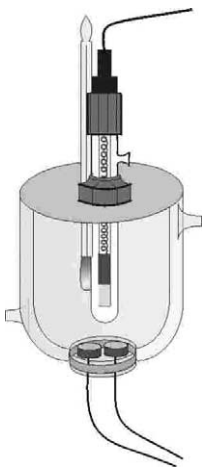

Fig. 1. Measurement cell.

2.2. Instrumentation and ENM set-up

A 1287SI electrochemical interface controlled by CorrWare software was used to measure both potential and current noise signals simultaneously at open circuit. The time records were acquired at a sampling rate of 2.15 points per second for about 15 min so that each register contains 2048 data points. The samples were exposed to the test solution for 4 days in order to follow the time evolution of the systems. The first EN time record was taken after 1 h of exposure. However, in order to reduce the amount of data to be handled and the scattering in the study of the evolution of the system, just six consecutive voltage and current time records were taken every 10 h. Thus, only an average value of each parameter will be provided for each series of consecutive time records.

2.3. Data treatment

In this section, two mathematical tools that have recently been proposed for the study of EN [14–16] are introduced, and these have been found very useful for the analysis of the experimental data obtained in this study.

2.3.1. Robust statistical parameters

The corrosion potential evolution can be studied to obtain information on corrosion processes [17,18]. This evolution will be estimated from the voltage records as the median value, as suggested in [14]. The median has been chosen because it provides a satisfactory estimate of the baseline of the signals, especially for the asymmetric signals usually produced by voltage noise when a localised corrosion process occurs.

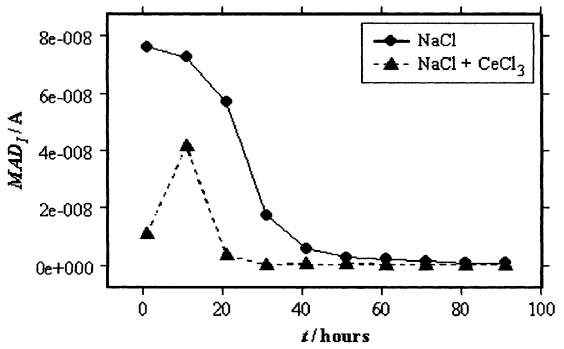

Fig. 2. Time evolution of MAD_I obtained for AA5083 alloy samples exposed to the indicated solutions.

Standard deviation is one of the simplest parameters for measuring the magnitude of fluctuation in electrochemical noise [18,19]. However, there is a robust statistical parameter that yields a better estimate of the range of fluctuation when the time record studied, x_i, is asymmetric: the median absolute deviation, or MAD:

$$\mathrm{MAD}_{x_i} = 1.4826 \ \text{median}\ (|x_i - \text{median}\ (x_i)|) \quad (1)$$

This parameter can be used in the same terms as standard deviation to evaluate corrosion activity [14].

The noise resistance, R_n, is defined as the ratio of a second-order statistics of the voltage fluctuations divided by the same quantity relative to the current fluctuations [20]. If this second-order statistic is the standard deviation, the difference in skew of voltage and current signals will affect the value of R_n [14]. To reduce this problem, in this paper, the noise resistance will be calculated as

$$R_n = \frac{\mathrm{MAD}_V}{\mathrm{MAD}_I} \quad (2)$$

2.3.2. Energy distribution plot (EDP)

One of the most frequently used methods to analyse EN consists of studying power spectral density (PSD) plots, which are calculated by means of Fourier transform. These plots provide information on the shape of the time record, which is supposed to be related to the corrosion mechanism [21,22]. However, it has been found recently that wavelet transform might improve the Fourier transform result when studying EN [15]. Specifically, a new kind of representation, energy distribution plot (EDP), has been suggested; this can be used as 'fingerprints' of signals, in a similar way to PSD plots. These representations were used in [16] to characterise and distinguish time records where PSD plots fail.

To represent an EDP of a signal x_n, $n = 1, 2, \ldots, N$, it is necessary to calculate the wavelet transform of the signal. From this operation, N wavelet coefficients are obtained ordered in $J+1$ vectors, termed crystals:

$$d_1 = (d_{1,1}, d_{1,2}, \ldots, d_{1,N/2}), \quad d_2 = (d_{2,1}, d_{2,2}, \ldots, d_{2,N/4}), \ldots,$$
$$d_j = (d_{j,1}, d_{j,2}, \ldots, d_{j,N/2^j}), \ldots$$
$$d_J = (d_{J,1}, d_{J,2}, \ldots, d_{J,N/2^J}), \quad s_J = (s_{J,1}, s_{J,2}, \ldots, s_{j,N/2^J})$$

where J is chosen from 1 to a maximum value. This maximum value depends on N and other characteristics of the specific wavelet transform applied. The results shown here have been calculated in the same way as in [16] and using the maximum value of J, which is 8.

Each crystal yields a description of the signal fluctuation at different temporal scale, so that the greater the fluctuation in the signal at a given scale, the higher the wavelet coefficients in the crystal that describes that scale. Thus, the subscript of the crystal name, j, defines the scale to which the crystal refers. The scale range which is taken into account for each crystal can be computed roughly from the following equation:

$$(C_1^j, C_2^j) = (2^j t_s, 2^{j-1} t_s) \quad (3)$$

where t_s is the sampling interval of the original signal.

One way of showing the results of the wavelet transform can be to estimate the contribution of each crystal to the overall signal, which can be performed through the fraction of energy associated with each crystal:

$$E_j^d = \frac{\sum_{n=1}^{N/2^j} d_{j,n}^2}{\sum_{n=1}^{N} x_n^2} \quad E_J^s = \frac{\sum_{n=1}^{N/2^J} s_{J,n}^2}{\sum_{n=1}^{N} x_n^2} \qquad j = 1, \ldots, J \quad (4)$$

Thus, an EDP is defined as the representation of the relative energy accumulated by each crystal versus the crystal name.

3. Results and discussion

3.1. Statistical study

In this section, the behaviour of alloy AA5083 in artificial seawater is compared with its behaviour when this solution is doped with an inhibitor ($CeCl_3$ at 500 ppm). To illustrate the behaviour of the alloy in both environments, the parameter MAD_I at different exposure times is shown in Fig. 2. In this figure, higher values of MAD_I indicate higher activities in the WEs. It is notable that the MAD_I data indicate that the activity is always lower when there is Ce^{3+} in the solution. In the absence of inhibitor, the magnitude of the fluctuations decreases as the time elapses, especially after about 1 day of immersion. Further, a maximum of MAD_I is observed at different exposure times depending on the system: at the beginning of the experiment for the solution without inhibitor, and after 11 h when there is Ce^{3+} in the medium. On the other hand, there is a time evolution so that the two systems tend to show

almost the same MAD_I values at the end of the experiment. Thus both systems undergo a similar activity after an 80 h exposure.

Another interesting property of the systems is the difficulty encountered by each interface in transferring charge, which is reflected in the noise resistance values. Fig. 3 shows the noise resistance evolution for the two systems, which has been calculated using Eq. (2). As might be expected, R_n is higher after any time of exposure when the solution contains inhibitor, which bears out the inhibitor effect of the Ce^{3+}. Furthermore, for the system without inhibitor, the resistance increases with the time, which explains the reduction in activity observed in Fig. 2. However, although there is a coincidence between the maximum MAD_I and the minimum R_n values for the system with inhibitor, it is not possible to find such correspondence in Fig. 2 with the high values of R_n obtained after 31 and 51 h of immersion. This might be because the system with inhibitor involves complex processes that cannot be evaluated solely from these parameters. From Fig. 3 it can be seen that, at the end of the period of time of the study, R_n is much higher for the system with inhibitor.

In order to understand the differences in behaviour of the systems with and without inhibitor, the median of the voltage noise, V_m, recorded at different exposure times has been plotted in Fig. 4. In this figure, it can be

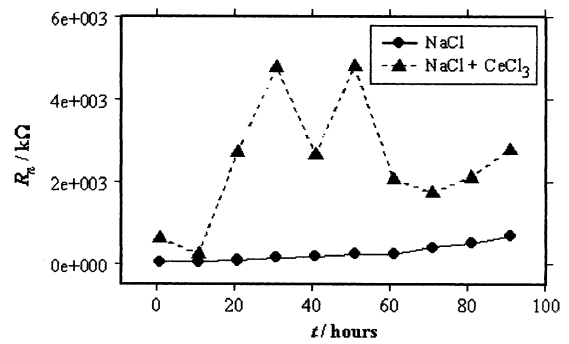

Fig. 3. Time evolution of R_n obtained for AA5083 alloy samples exposed to the indicated solutions.

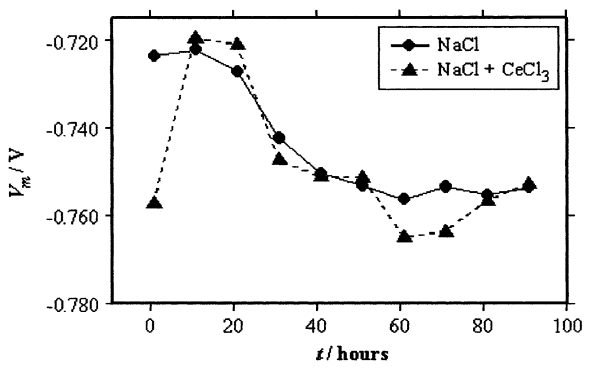

Fig. 4. Time evolution of V_m obtained for AA5083 alloy samples exposed to the indicated solutions.

observed that there are two potentials towards which both systems have a tendency. Those potentials are about -720 mV at the beginning of the experiment and about -755 mV afterwards. It should be noticed that the potential does not increase above the pitting potential of the alloy obtained through potentiodynamic tests [6]. The main corrosion process occurring when the potential is about -720 mV must be crystallographic pitting. This process develops causing the anodic processes and repassivation to be alternated, producing the electrochemical noise. However, after the 1st day of exposure, both systems evolve so that their potential is about -755 mV, which indicates that crystallographic pitting has stopped, and gives way to alkaline pitting [6]. However, those processes would take place to a much lesser extent when there is Ce^{3+} in the medium, as Figs. 2 and 3 suggest.

The potential decrease observed in Fig. 4 for both systems implies the increase of the ratio of anodic rate to cathodic rate. However, an increase in the anodic rate is not expected because MAD_I decreases in the period of time in which V_m decreases. Therefore, it is a sensible assumption that the cathodic reaction takes place with more dificulty as time elapses. The origin of the decrease in the cathodic reaction rate must be different for each system. Thus, in accordance with [1,4], when there is no inhibitor in the medium, the dissolution of the matrix around the Al(Mn, Fe, Cr) particles would cause the successive detachment of these particles and therefore, since those intermetallic particles facilitate the cathodic reaction, this takes place progressively more slowly. However, if there is Ce^{3+} in the solution, the Al(Mn, Fe, Cr) particles are progressively blocked because of the inhibitor effect of the lanthanide cation [9]. It is noticed that, although the activity of both systems decreases with time, Fig. 2, this occurs at the expense of damaging the surface of the alloy when cerium cations are not present in the medium. The inhibition effect can be observed in Fig. 5 where images of the surface of AA5083 samples exposed to a 3.5% NaCl solution and a 3.5% NaCl solution + $CeCl_3$ at 500 ppm solution are shown.

Although not shown in Fig. 4, the potential of the WEs in the solution without inhibitor was about -850 mV at the very beginning of the experiment. Hence, there is a very steep increase in the potential during the first hour. Moreover, in the presence of Ce^{3+}, another increase in potential is also observed at the beginning of the experiment, but this is much slower. Both increases might be caused by the growth of the oxide layer over the alloy matrix. However, the process appears to be much slower when there is Ce^{3+} in the medium. Probably, this delay is a consequence of the blockage of the cathodic reaction, which hinders the oxide film formation as well. Paradoxically, this delay causes the crystallographic pitting to start later, which is also reflected in

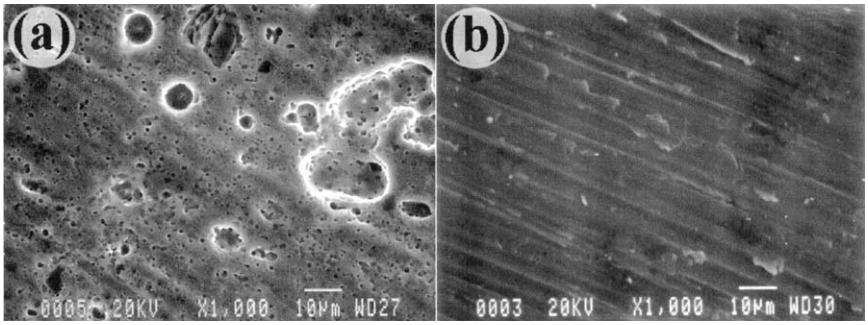

Fig. 5. Images of the surface of AA5083 samples exposed to: (a) 3.5% NaCl solution; and (b) 3.5% NaCl solution + $CeCl_3$ at 500 ppm solution, both for 30 days.

Fig. 2, showing that the activity when there is Ce^{3+} in the medium is relatively low after a hour of exposure time. Moreover, it has been observed in previous studies [23] that passive layers formed in the presence of Ce^{3+} are more protective. This fact is also reflected in the higher R_n obtained for the system with Ce^{3+} in the medium once the oxide film has developed sufficiently.

3.2. Wavelet study

Until now, this paper has only dealt with the magnitude of the fluctuations in the EN records. However, other characteristics of the time records could provide information on the corrosion mechanism. One of these characteristics may be the time scale of fluctuations appearing in the time records. As mentioned in Section 2.3.2, this feature of the time records can be quantified by using EDPs.

Fig. 6 shows a series of EDPs that have been linked to form a three-dimensional diagram. Each of the EDPs describes a current time record registered at a different exposure time for the system without inhibitor. This figure allows three stages to be distinguished in regard to the shape of the current time record for the system without inhibitor. In Fig. 7 the differences between the three stages can be seen clearly, since an EDP for each stage has been plotted in a two-dimension graph. To illustrate the meaning of these stages, a representative current time record of each stage detected in Fig. 6 is shown in Fig. 8. The first stage concerns the two first measurements (after 1 and 11 h of exposure), which were characterised by time records whose energy is mainly spread among the crystals d_1–d_5. This means that their fluctuations have a variety of constant times, but they are mainly short, Fig. 8(a). The second stage corresponds to measurements after 21 and 31 h of immersion. The main feature of this stage is the existence of a large-scale component, Fig. 8(b), reflected in the high values of energy for crystal s_8. Subsequently, the system seems to stabilise concentrating its energy on the crystals d_4–d_6. These crystals are those that correspond to the time scale of the transients present in time records like the one in Fig. 8(c).

Taking into account the results of Figs. 2–4, there appears to be a correlation between the mechanism of

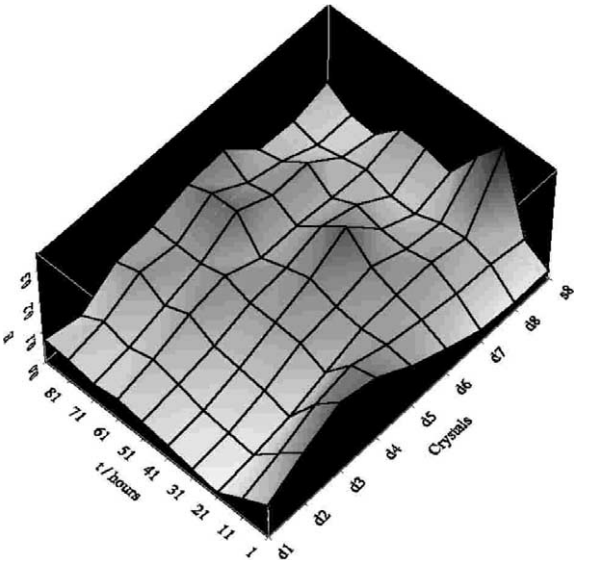

Fig. 6. Time evolution of current EDPs obtained for AA5083 alloy samples exposed to a 3.5% NaCl solution.

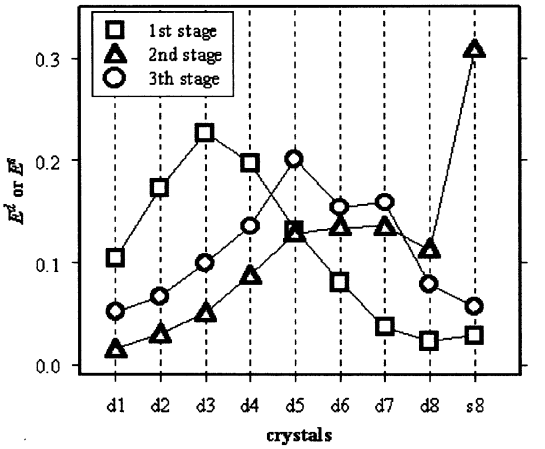

Fig. 7. EDPs representative of each of the stages detected in Fig. 6.

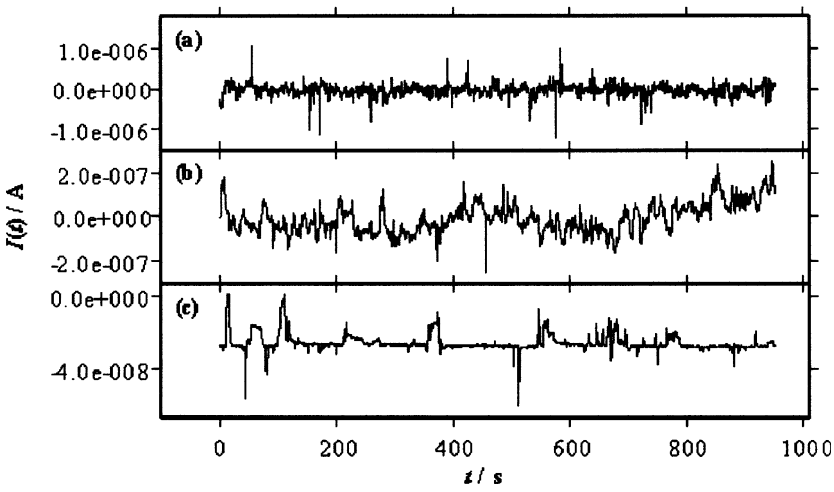

Fig. 8. Current time records obtained for AA5083 alloy samples exposed to a 3.5% NaCl solution for: (a) 1 h; (b) 21 h; and (c) 91 h.

evolution proposed in Section 3.1 and the three stages observed in Fig. 6. Hence, the first stage would correspond to the prevalence of crystallographic pitting, the third stage to the development of alkaline pits while the intermediate second stage is a transition between the two stages.

The three-dimensional EDP of the system with inhibitor is plotted in Fig. 9. Unlike Fig. 6, it is difficult, in Fig. 9, to divide the evolution of the energy distribution into distinct stages. This might be due to the fact that the evolution of the system with inhibitor is much more complex, as was already observed from the results in Figs. 2–4. On the other hand, it can be seen that Fig. 9 differs notably from Fig. 6. In general, the energy of current time records accumulates at crystals of shorter scale for the system with Ce^{3+} than for the system without the inhibitor. This fact could be correlated with the transient duration for the two systems. Fig. 10 shows a current time record made at the same exposure time as the one in Fig. 8 (c), i.e. 91 h. By comparing these figures, it can be observed that the transient duration is lower when the solution contains Ce^{3+}. Furthermore, the transients present in Fig. 8 (c) are composed of several peaks, which suggests that the transients are related to a pit development that grows by means of several short-duration events. However, when there is Ce^{3+} in the medium, overlapped transients are infrequent. This suggests that once a first event initiates the corrosion process, the Ce^{3+} action blocks the development of the pit.

3.3. Transient shape study

There is a feature in some transients that appears when the solution contains Ce^{3+}, which deserves special attention. This peculiarity consists of an unusual coupling between transients so that a sudden current transient in one direction is often accompanied by a slower and smaller current transient in the opposite direction. These transients seem to be a consequence of the same phenomenon because they often appear together and associated with just one voltage transient, as in the example plotted in Fig. 11.

The shape of the coupled transients seems to provide information on the mechanism whereby the Ce^{3+} cations inhibit the alkaline pitting. Thus, we shall consider the two WEs involved in the measurement: Electrode 1 and 2. If, for instance, part of the alloy matrix around an Al(Mn, Fe, Cr) particle is oxidising in Electrode 1, an excess of electrons is produced in this electrode. However, since both WEs are connected through a ZRA, the charge is split equally between the two WEs. In fact, the first current transient in Fig. 11 is a consequence of the flow of half the charge produced

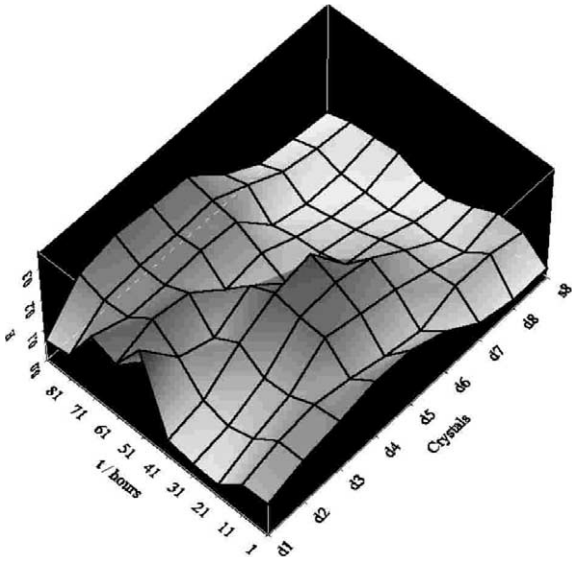

Fig. 9. Time evolution of current EDPs obtained for AA5083 alloy samples exposed to a 3.5% NaCl solution + $CeCl_3$ at 500 ppm.

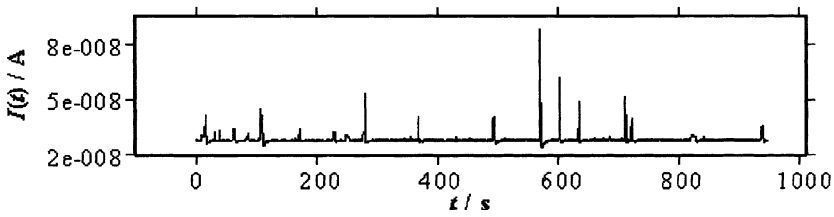

Fig. 10. Current time record obtained for AA5083 alloy samples exposed to a 3.5% NaCl solution + $CeCl_3$ at 500 ppm for 91 h.

in Electrode 1 to 2. Moreover, this anodic process would decrease the potential as shown in Fig. 11. Subsequently, this excess of electrons is normally consumed by cathodic reactions taking place in both WEs equally, which leads to a potential increase without any current transient associated with the same phenomenon. However, this does not seem to be the case for the AA5083 when the medium contains Ce^{3+}. A second current transient occurs, without the appearance of a voltage transient (Fig. 11). Hence, since the second current transient occurs just after the first one and in the opposite direction, it appears that the excess of electrons is reorganised so that part of the charge transferred to the Electrode 2 reverts to Electrode 1. Such behaviour can be explained if Electrode 1 has a special facility to consume electrons. If this is so, and since in principle the two WEs are identical, the cathodic reaction must occur preferentially in Electrode 1, where alkaline attack took place. On the other hand, this phenomenon has not been observed when there is no Ce^{3+} in the solution. Therefore, the inhibitor must play an important role in the explanation of the second transient. Specifically, the result in Fig. 11 supports the notion of an inhibition mechanism in which the Ce^{3+} cations precipitate onto the Al(Mn, Fe, Cr) particles especially when a matrix dissolution happens. This precipitation would involve the consumption of OH^- anions, which encourages the formation of further OH^- anions in Electrode 1, through the consumption

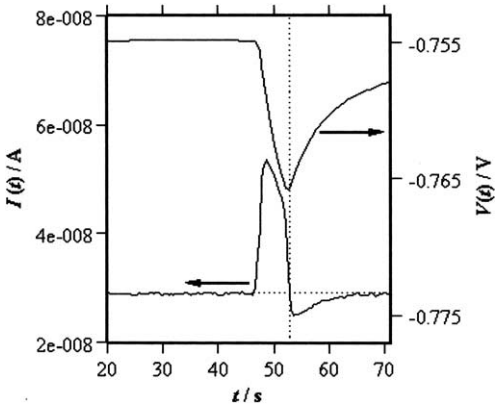

Fig. 11. Current and voltage time records obtained for AA5083 alloy samples exposed to a 3.5% NaCl solution + $CeCl_3$ at 500 ppm for 81 h. Detail of a transient.

of electrons observed experimentally. Thus the observation of transients like the ones shown in Fig. 11 can be used to identify when an inhibition event is occurring.

4. Conclusions

The study of the evolution of EDP versus time provides a convenient way of considering the changes over the time in the shape of the EN records as well as a way of comparing the progress of the mechanism in the two systems. In this study, EDP has been used to study the corrosion behaviour of alloy AA5083 exposed to a 3.5% NaCl solution with and without Ce^{3+} as inhibitor. The corresponding EDPs were useful in detecting that, in general, transients are shorter when there is Ce^{3+} in the medium, which might be a consequence of a faster repassivation of the pit. In addition, it was possible to investigate whether the system studied suffered changes in the structure of the noise records.

The evolutions of free potential, current noise and resistance noise have been studied by means of robust parameters suggested in [14]. The voltage median evolution of AA5083 aluminium samples exposed to a 3.5% NaCl solution suggests that the main corrosion process is crystallographic pitting for about the 1st day, but alkaline pitting later. However, a study of the noise fluctuation magnitude indicates that the activity was much lower in the presence of Ce^{3+} at all times, but especially for the 1st day of exposure. In addition, the corrosion activity decreases with time for both systems. Nevertheless, the origin of this decrease in activity was the loss of intermetallic particles from the alloy surface when there is no Ce^{3+} in the medium, while its origin was the blockage of these particles when the solution contains inhibitor. A side effect of the inhibitor is to delay the formation of the passive layer, which, paradoxically, prevents the formation of crystallographic pits.

From the shape of transients recorded when samples of alloy AA5083 are undergoing alkaline pitting in a 3.5% NaCl solution + 500 ppm Ce^{3+}, it seems that the Ce^{3+} cations hinder alkaline pitting, not only by precipitating onto the Al(Mn, Fe, Cr) before the attack starts, but also by precipitating while the attack is in progress.

Acknowledgements

This work has received financial support from the Junta de Andalucía and la Comisión Interministerial de Ciencia y Tecnología (CICYT), projects MAT99-0625-C02-01 and 1FD97-0333-C03-02.

References

[1] M. Bethencourt, F.J. Botana, J.J. Calvino, M. Marcos, J. Pérez, M.A. Rodríguez-Chacón, Mater. Sci. Forum 298–292 (1998) 567.
[2] A.J. Aldykewicz, H.S. Isaac, A.J. Davenport, J. Electrochem. Soc. 143 (1996) 147.
[3] K. Nisancioglu, J.K. Davanger, O. Strandmyr, J. Electrochem. Soc. 137 (1990) 69.
[4] A. Aballe, M. Bethencourt, F.J. Botana, J. Cano, M. Marcos, Corros. Rev. 18 (1) (2000) 1.
[5] Ph. Giménez, J.J. Rameau, M.C. Rebioul, Corrosion 37 (1981) 673.
[6] A. Aballe, M. Bethencourt, F.J. Botana, M.J. Cano, M. Marcos, Corros. Sci. 43 (2001) 1657.
[7] B.R.W. Hinton, D.R. Arnott, N.E. Ryan, Metal Forum 7 (4) (1984) 11.
[8] A. Aballe, M. Bethencourt, F.J. Botana, M.J. Cano, M. Marcos, Mater. Corros. 52 (5) (2001) 344.
[9] M. Bethencourt, F.J. Botana, J.J. Calvino, M. Marcos, Corros. Sci. 40 (1998) 1803.
[10] M.A. Arenas, M. Bethencourt, F.J. Botana, J. Damborenea, M. Marcos, Corros. Sci. 43 (2001) 157.
[11] A. Aballe, M. Bethencourt, F.J. Botana, M. Marcos, J. Pérez, M.A. Rodríguez-Chacón, Mater. Sci. Forum 289–292 (1998) 557.
[12] M. Bethencourt, F.J. Botana, M. Cauqui, M. Marcos, M. Rodríguez, J. Rodríguez, J. Alloys Comp. 250 (1997) 455.
[13] A. Aballe, M. Bethencourt, F.J. Botana, M. Marcos, J. Alloys Comp. 323–324 (2001) 855.
[14] A. Aballe, PhD Thesis, University of Cádiz, 2001.
[15] A. Aballe, M. Bethencourt, F.J. Botana, M. Marcos, Electrochem. Commun. 1/7 (1999) 266.
[16] A. Aballe, M. Bethencourt, F.J. Botana, M. Marcos, Electrochim. Acta 44 (1999) 4805.
[17] J.R. Kearns, D.A. Eden, M.R. Yaffe, J.V. Fahey, D.L. Reichert, D.C. Silverman, in: J.R. Kearns, J.R. Scully, P.R. Roberge, D.L. Reichert, J.L. Dawson (Eds.), Electrochemical Noise Measurement for Corrosion Applications, ASTM, West Conshohocken, 1996, pp. 446–470.
[18] F. Mansfeld, H. Xiao, J. Electrochem. Soc. 140 (1993) 2205.
[19] P.C. Pistorius, in: J.R. Kearns, J.R. Scully, P.R. Roberge, D.L. Reichert, J.L. Dawson (Eds.), Electrochemical Noise Measurement for Corrosion Applications, ASTM, West Conshohocken, 1996, pp. 343–358.
[20] U. Bertocci, C. Gabrielli, F. Huet, M. Keddam, J. Electrochem. Soc. 144 (1997) 31.
[21] D.A. Eden, Proc. Corrosion/98, paper 386, NACE, Houston, 1998.
[22] U. Bertocci, F. Huet, B. Jaoul, P. Rousseau, Corrosion 56 (2000) 675.
[23] A. Aballe, M. Bethencourt, F.J. Botana, M.J. Cano, M. Marcos, Mater. Corros. 52 (2001) 1.